Inorganic Chemistry

Article

pubs.acs.org/IC

Chemical Bonding in a Linear Chromium Metal String Complex

Lai-Chin Wu,[†] Maja K. Thomsen,[†] Solveig R. Madsen,[†] Mette Schmoekel,[†] Mads R. V. Jørgensen,[†] Ming-Chuan Cheng,[‡] Shie-Ming Peng,[‡] Yu-Sheng Chen,[§] Jacob Overgaard,*[,†] and Bo B. Iversen*[,†]

[†]Center for Materials Crystallography, Department of Chemistry and iNANO, Aarhus University, Langelandsgade 140, Aarhus DK-8000, Denmark

[‡]Department of Chemistry, Academia Sinica, Taipei, Taiwan

[§]ChemMatCARS Beamline, Advanced Photon Source, The University of Chicago, Argonne, Illinois 60439, United States

Supporting Information

ABSTRACT: A combined experimental and theoretical electron density study of the shortest trichromium metal wire, $Cr_3(dpa)_4Cl_2\cdot(C_2H_5OC_2H_5)_x(CH_2Cl_2)_{1-x}$ (**1**, dpa = bis(2-pyridyl)amido), is reported. High resolution X-ray diffraction data has been collected both at 100 K using a conventional X-ray source (DS1) and at 15 K using a synchrotron X-ray source (DS2). The linear chromium string is terminated by Cl^- ions at both ends, and each Cr atom is also coordinated by four N atoms from bridging dpa ligands. The two Cr−Cr bond distances are unequal at 100 K (with d(Cr1−Cr2) being 0.029 Å shorter than d(Cr2−Cr3)) but at 15 K they are almost equal (0.002 Å difference). Analysis of the slightly elongated thermal ellipsoids of the Cr2 atom suggests that it is not due to disorder, but the presence of a shallow potential energy surface. Laplacian maps clearly show local valence shell charge concentration (VSCC) in the electron density along the bisector of the equatorial Cr−N bonds. Integration over the atomic basins indicates that Cr2 has smaller atomic charge and volume than Cr1 and Cr3. The topological characterization of the Cr−Cr bonds indicates partly covalent characters with electron density at the bond critical point of ∼0.3 e Å^{-3} and negative total energy density. The delocalization index of Cr−Cr is 0.8 for Cr1−Cr2 and 0.08 for Cr1−Cr3. Second-order perturbation analysis shows high stabilization energy of the Cr−Cr bonds (E(2) ∼ 190 kcal mol^{-1}). Delocalization indices and source function and natural bond orbital analyses are all indicative of localized Cr−Cr bonding interactions.

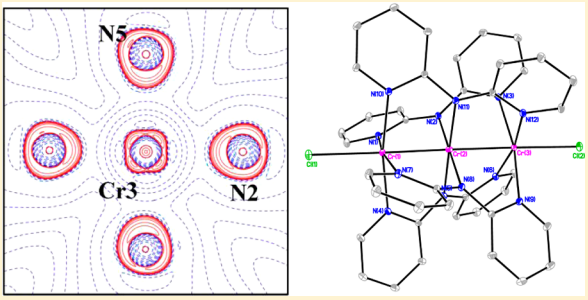

INTRODUCTION

Linear metal string complexes (oligo-α-pyridylamido based), or so-called extended metal atom chain complexes (EMAC), have been studied for decades due to their potential applications as molecular wires.[1] The electrical conductivity of EMACs, such as $M_nL_4(NCS)_2$ where M = Cr, Co, and Ni, n = 3 (L = bis(2-pyridyl)amido, dpa), n = 5 (L = tris(pyridyl)diamido), and n = 7 (L = tetra(pyridyl)triamido), has been studied by STM,[2−4] and the conductivity increases in the order of Ni, Co, and Cr. This correlates well with results from extended Hückel molecular orbital calculations showing an increasing metal−metal formal bond order of 0, 0.5, 1.5 along this series.[3] This indicates that the nature of the metal−metal bond plays an important role in the conductance of the metal wires.[4]

Three-membered metal string complexes, $M_3(dpa)_4X_2$ (M = Cu,[5−9] Ni,[9−16] Co,[17,18] Cr[19−25]) are obviously the shortest strings possible. The most interesting of these materials are $Cr_3(dpa)_4X_2$[19−21,23,24,26] and $Co_3(dpa)_4X_2$[17,18] because they exist both as symmetric (s-form) and unsymmetric (u-form) molecular structures. In the case of trichromium chains, tuning of the two Cr−Cr bond distances can be achieved by the choice of axial ligands.[20,21] Most types of ligands (weak or intermediate ligand, such as Cl^-, Br^-, NCMe) provide the u-form while strong σ donor ligands (such as CN^-, CCPh) lead to the s-form. The Cr−Cr bond distances of the s-form[19−22] are roughly 2.36 Å while the u-form has bond distances in the range 2.2−2.5 Å.[20,21] When the axial ligands are Cl^- ions, the molecule can be symmetric with a center of inversion on the central Cr atom (Cr2), i.e., with CH_2Cl_2 as solvent the Cr−Cr bond distance is 2.366 Å, whereas it is 2.365 Å with tetrahydrofuran. Alternatively, the molecule is unsymmetric when benzene (d(Cr−Cr) of 2.326 and 2.390 Å) or toluene (2.353 and 2.365 Å) is used as solvent. These cases represent quite small differences of Cr−Cr bond distance, but significantly more unsymmetric structures are observed when the axial ligands at the two ends differ, such as the combination of BF_4^- and Cl^- (1.995 and 2.643 Å) or PF_6^- and Cl^- (2.008 and 2.614 Å). The molecular spin states of both the symmetric and the unsymmetric compounds are found by magnetic measurements,[20] and supported by theoretical calculations,[26−29] to be quintet states (S = 2) with antiferromagnetic coupling between Cr atoms. According to theory (gas phase molecular calculations), the symmetric structure has the lowest energy, and the atomic spin population of each Cr atom is 3.5 for terminal Cr atoms and −3.0 for the central atom (with negative

Received: August 9, 2014
Published: November 10, 2014

   dx.doi.org/10.1021/ic501603x | Inorg. Chem. 2014, 53, 12489−12498

sign indicating opposite spin direction). In the unsymmetric case (Δd_{Cr-Cr} = 0.106 Å), the energy is 0.97 kcal mol^{-1} higher than the symmetric one, and the atomic spin populations of the Cr atoms are 3.60, −3.00, and 3.44.[26] In the case of $Co_3(dpa)_4Cl_2$, theory also predicts the symmetrical structure to be the ground state.[27−29] In general, it is not clear how much the bonding in the molecular structure is perturbed by supramolecular effects (i.e., crystal effects). In the case of $Co_3(dpa)_4Cl_2$ a symmetrical structure is observed if the molecule is crystallized with one solvent CH_2Cl_2 molecule, whereas the presence of two solvent CH_2Cl_2 molecules in the crystal results in an unsymmetrical structure.[18]

Apart from direct observation in crystal structures, the s- and u-forms of $Cr_3(dpa)_4Cl_2$ can also be identified by IR and surface-enhanced Raman spectroscopy (SERS).[23,24] The s-form exhibits a Cr−Cr−Cr asymmetric stretching band at 346 cm^{-1} in IR, and the u-form shows a Cr−Cr quadruple bond stretching band at 570 cm^{-1} in Raman spectra. The two forms are thermally accessible by interconversion in solution when the temperature is above 60 °C.[23] The observed enthalpy and entropy of this reaction, calculated from temperature dependent SERS, are ΔH = 46.2 kJ mol^{-1} and ΔS = 138 JK^{-1} mol^{-1}, respectively. These values are consistent with the relative energy difference between the symmetric ground state and unsymmetric excited state, and the experimentally observed thermal conversion of the two forms.

In this work we take a different approach to study the electronic structure of an EMAC. Bader's quantum theory of atoms in molecules (QTAIM)[30] provides a concept for characterizing chemical interactions in terms of the electron density, and a range of descriptors have been developed to assess the nature of chemical bonds. The existence of a bond critical point (BCP) and associated bond path are the criteria for any two interacting atoms. Chemical bonding can be categorized by the evaluation of topological properties at the BCP such as the electron density, ρ_b, the Laplacian of the density, $\nabla^2\rho_b$, the total energy density, H_b, and the ratio of the absolute value of the potential energy density to the kinetic energy density, $|V_b|/G_b$.[30−32] Pure shared shell (covalent) interactions have negative $\nabla^2\rho_b$ and H_b, and $|V_b|/G_b > 2$, whereas pure closed shell (ionic) interactions have positive $\nabla^2\rho_b$ and H_b, and $|V_b|/G_b < 1$. Transit closed shell interactions with positive $\nabla^2\rho_b$, negative H_b, and $1 < |V_b|/G_b < 2$ are typically seen in metal−ligand and metal−metal bonds.[31] Applications of QTAIM to metal−metal bonded dinuclear transition metal complexes are abundant in the literature,[33−49] and the metal−metal bond has been classified on the basis of topological properties at the BCP.[50] Generally, for a metal−metal bond, including both the relatively weak Mn−Mn bonding[36] and the strong Cr−Cr quintuple bond,[33] $|V_b|/G_b$ will be in the range 1.0−2.0. Although it is formally classified as a transit closed shell interaction, the Cr−Cr quintuple bond is considered as a covalent bond due to its large ρ_b, negative value of total energy value (H_b), and also the Fermi-hole distribution supports the existence of a quintuple bond.[33] In the present study we investigate the chemical bonding in $Cr_3(dpa)_4Cl_2$ using QTAIM based on both experimental and theoretical electron densities. In addition we apply the source function (SF)[50,51] and natural bond orbital (NBO) analyses to describe the chemical bonding.

EXPERIMENTAL SECTION

Synthesis. The synthesis of the trichromium linear metal string complex $Cr_3(dpa)_4Cl_2$ (**1**) was carried out following the procedures of Li et al.[52] The resulting powder was purified by recrystallization from a solution of dichloromethane with ether diffusion at room temperature. Dark green crystals, which were suitable for X-ray diffraction, were obtained after several days.

100 K Conventional X-ray Diffraction Data (DS1). A dark green crystal with dimensions 0.32 × 0.32 × 0.30 mm^3 was fixed with paratone-N oil on the tip of a glass fiber. This was attached to a brass pin, arranged on a goniometer head, and placed in a Bruker-Nonius APEXII diffractometer. A total of six series of data were collected at a crystal temperature of 100(1) K generated by an Oxford Cryosystems Cryostream Plus liquid N_2 cooling device. Using the program SAINT+,[53] a total of 297 409 (R_{int} = 0.0252) integrated intensities corrected for Lorentz and polarization effects were obtained. The intensities were corrected for absorption with the empirical method of SADABS,[54] giving minimum and maximum transmission coefficients of 0.75 and 0.76, respectively. Scaling and merging using SORTAV[55] resulted in 45 764 unique reflections. The data set was virtually complete (99.4%) to a resolution of sin θ/λ = 1.09 (0.46 Å).

15 K Synchrotron X-ray Diffraction Data (DS2). A small, dark green single crystal (0.110 × 0.066 × 0.052 mm^3) was mounted on the tip of a glass fiber with paratone-N oil. This assembly was mounted on a brass pin, which was placed on the goniometer of a modified APEXII diffractometer at the ChemMatCARS beamline (15 ID-B) at the Advanced Photon Source, Argonne National Laboratory, IL. The crystal was cooled to 15(1) K using the cold He stream from a Pinkerton type cooling device.[56] The data collection was done in ϕ-scan mode with fixed ω and χ angles. The diffracted intensities were recorded with a Bruker APEXII CCD detector up to a highest resolution of 1.25 Å^{-1} (d = 0.4 Å). The intensities were integrated using SAINT+ (759 946 integrated intensities),[53] which also provides a correction for the oblique incidence in the CCD phosphor.[57,58] Absorption correction was performed with SADABS,[54] whereas scaling and merging were done by SORTAV giving 66 068 unique reflections. The overall completeness is 96.2% with R_{int} = 0.0730, but the data set is virtually complete to a resolution of 1.0 Å^{-1}.

Electron Density Modeling. Identical procedures were used for the two data sets to refine structure and multipole parameters. The crystal structure was independently solved for each data set using the direct methods program SHELXS-97.[59] All non-hydrogen atoms were initially located, and subsequently their positions as well as anisotropic atomic displacement parameters (ADPs) were refined using the program SHELXL-97.[59] All hydrogen atoms of the dpa ligand were generated according to the ideal geometry (sp^2 or sp^3) of the connected atoms. Full-matrix least-squares refinement on F^2 was applied using observed reflections ($I > 2\sigma(I)$). The solvent ether and dichloromethane (DCM) molecules in unison occupy the rather large empty space between the $Cr_3(dpa)_4Cl_2$ molecules, and they exhibit both positional and dynamical disorder. The occupancies of the solvent molecules were freely refined but constrained to add up to 1. Interestingly, the occupancies of the solvent molecules vary from crystal to crystal, even for crystals within the same batch. The final values of the occupancies of ether and dichloromethane were 0.880(1) and 0.120(1) for DS1, and 0.9432(7) and 0.0568(7) for DS2, respectively.

For the multipole refinement, the independent atom model (IAM) from SHELXL was imported into the multipole refinement package XD2006.[60] The Hansen−Coppens multipole model[61] was used to analytically describe the nonspherical electron density. The local coordinate systems of the Cr atoms were defined with the z-axis pointing along the Cr−Cr direction, and the x- and y-axes pointing to the bisection of the Cr−N bonds. The electron configuration of the Cr atom was presumed to be [Ar]4s^{1}3d^5 with an Ar core and 3d^5 at valence shell. The one 4s electron was considered in different models as either valence or core, and it provided no improvement in the modeling in terms of R factors and residual density.[62] In the final model it was considered to be part of the core. The scattering factors used for all atoms were obtained from STO relativistic wave functions (the VM data bank). First, a high-order refinement was performed on the structural parameters of all non-hydrogen atoms (all differences of mean-square displacement amplitudes, DMSDAs, except for the Cr−Cr bonds, are in the range of 0.0001−0.001 Å^2, see Supporting Information for

dx.doi.org/10.1021/ic501603x | Inorg. Chem. 2014, 53, 12489−12498

Table 1. Crystallographic Data and Refinement Results

	DS1	DS2
T (K)	100(1)	15(1)
wavelength (Å)	0.710 73	0.3936
cryst syst	monoclinic	monoclinic
space group	$P2_1/c$	$P2_1/c$
unit cell dimensions (Å)/ β in °	a = 16.0253(5)	a = 15.961(1)
	b = 15.7895(5)	b = 15.713(1)
	c = 17.0090(6)	c = 16.945(1)
	β = 98.799(2)	β = 98.948(3)
V (Å^3), Z	4253.2(2), 4	4198.1(5), 4
cryst size (mm^3)	0.32 × 0.32 × 0.30	0.11 × 0.07 × 0.05
θ range for data collection (°)	1.29−50.73	0.98−29.47
$(\sin(\theta)/\lambda)_{max}$ (Å^{-1})	1.09	1.25
reflns collected	297 409	759 946
indep reflns	45 764 [R(int) = 0.0252]	66 068 [R(int) = 0.0730]
completeness (%)	99.4	96.2
data/restraints/params	36 310/0/588	49 681/0/588
GOF on F^2	1.035	0.986
final R indices [$I > 2\sigma(I)$]	R1 = 0.0345, wR2 = 0.0936	R1 = 0.0293, wR2 = 0.0758
R indices (all data)	R1 = 0.0496, wR2 = 0.1033	R1 = 0.0489, wR2 = 0.0832
multipole model	R1 = 0.0255, wR1 = 0.0257	R1 = 0.0276, wR1 = 0.0239
	R2 = 0.0283, wR2 = 0.0508	R2 = 0.0372, wR2 = 0.0472
data included in the refinement	32 635	54 690
restraints[a]/params	132/1858	132/1858

[a]Positions of hydrogen atoms.

details). This was followed by a series of refinements with the level of multipoles increasing in stages. The final model included all multipoles up to hexadecapole level for the Cr and Cl atoms, and up to octupole level for the remaining non-hydrogen atoms. All hydrogen atoms are initially positioned by a riding model.[63] The bond distances to their nearest neighbors were fixed according to published neutron diffraction values,[64] and only the monopoles and bond-directed dipoles were refined. Identical κ parameters were used for Cr1 and Cr3, while a separate κ was used for Cr2. In addition one κ was used for each of the other atom types (Cl, O, N, C, and H). In the final refinement, all parameters (atomic positions, ADPs, multipole parameters and κ) were refined freely except the positions, ADPs, and multipole parameters of atoms of the solvent molecules, and quick convergence was achieved. During the refinement the $Cr_3(dpa)_4Cl_2$ molecule was constrained to be neutral; i.e., no charge transfer between solvent and main molecule was allowed. The topological properties of the bond critical points (BCP) and the Laplacian distributions were obtained with XD2006.[60] Details about the structural refinements are given in Table 1. CCDC 973959−973960 (for DS2 and DS1) contain the supplementary crystallographic data for this Article. These data can be obtained free of charge from The Cambridge Crystallographic Data Centre via www.ccdc.cam.ac.uk/data_request/cif.

Theoretical Calculations. Two different single point DFT calculations were carried out for **1** using Gaussian09,[65] one for each of the experimental geometries, DS1 and DS2. The unrestricted BP86[66−69] functional was used with the basis set cc-PVTZ[70] without g functions for Cr, 6-311G* for Cl, 6-31G* for N and C, and 3-21G for H, respectively. NBO analysis,[71−74] which provides the most probable Lewis structure picture, was subsequently applied. The donor−acceptor interactions in the NBO basis can be calculated by performing a second-order perturbation theory analysis. The donor is typically an occupied Lewis-type NBO(i), and the acceptor is typically an unoccupied non-Lewis-type NBO(j). The stabilization energy, $E(2)$, is related to the delocalization from the donor to the acceptor and is a measure of the strength of the interaction. The NBO analysis of **1** was performed by NBO 3.0.[75] Topological analysis of the DFT results was carried out using AIMALL.[76]

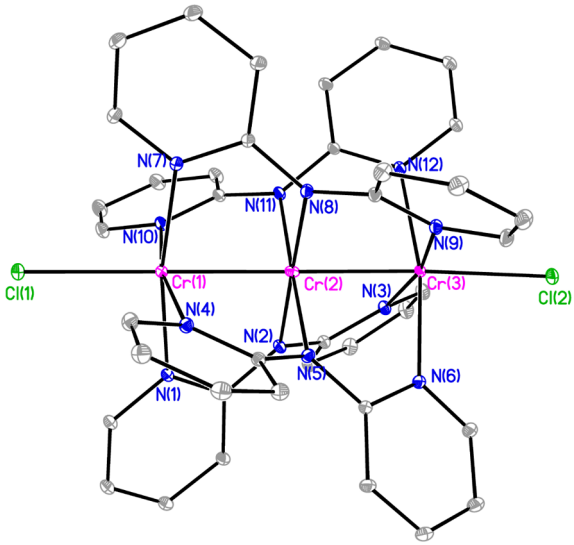

Figure 1. Molecular structure of **1** at 15 K plotted with 50% ellipsoids.

RESULT AND DISCUSSION

Structure Description. As mentioned above, the two Cr−Cr bond distances can be tuned by the proper choice of axial ligands.[20−22] The axial ligand of **1** is the Cl^- ion which is considered a weak ligand, and therefore, a u-form for the molecular structure is expected. As shown in Figure 1 the three chromium atoms are bridged by the four dpa ligands. Selected bond distances for **1** are shown in Table 2. To quantify the asymmetry in the metal−metal bond distances, the differences in bond distances between the two Cr−Cr bonds is used. In **1**, these amount to 0.029 and 0.002 Å for DS1 (100 K) and DS2 (15 K), respectively. This indicates that Cr2 is closer to the midpoint of Cr1···Cr3 at lower temperatures in agreement with theoretical calculation showing that the symmetric structure

dx.doi.org/10.1021/ic501603x | Inorg. Chem. 2014, 53, 12489−12498

Table 2. Selected Bond Distances (Å) of DS1 and DS2

bond	DS1, Å	DS2, Å	del,[a] Å	bond	DS1, Å	DS2, Å	del,[a] Å
Cr1−Cr2	2.3480(2)	2.3669(1)	0.019	Cr1−Cl1	2.5481(2)	2.5337(2)	−0.014
Cr2−Cr3	2.3773(2)	2.3689(2)	−0.008	Cr3−Cl2	2.5065(2)	2.4948(2)	−0.012
Δd_{Cr-Cr}[b]	−0.029	−0.002		Δd_{Cr-Cl}[b]	0	0	
Cr1−N1	2.1199(5)	2.1183(3)	−0.002	Cr2−N8	2.0327(5)	2.0305(3)	−0.002
Cr1−N4	2.1183(5)	2.1151(3)	−0.003	Cr2−N11	2.0331(5)	2.0298(3)	−0.003
Cr1−N7	2.1285(5)	2.1259(3)	−0.003	Cr3−N3	2.1017(5)	2.0978(3)	−0.002
Cr1−N10	2.1234(5)	2.1215(3)	−0.002	Cr3−N6	2.1262(5)	2.1233(3)	−0.003
Cr2−N2	2.0389(5)	2.0367(3)	−0.002	Cr3−N9	2.1204(5)	2.1174(3)	−0.004
Cr2−N5	2.0319(5)	2.0292(3)	−0.003	Cr3−N12	2.1100(5)	2.1063(3)	−0.003

[a]del = DS2 − DS1. [b]$\Delta d_{Cr-Cr} = d_{Cr1-Cr2} - d_{Cr2-Cr3}$.

should be the ground state.[26−29] The asymmetry at higher temperatures may be related to the thermal population of excited states. Comparing bond distances of DS1 and DS2, it is the Cr1−Cr2 bond distance that changes the most (0.019 Å), followed by the Cr−Cl distances (0.014 and 0.012 Å) and Cr2−Cr3 (0.008 Å). All Cr−N bond distances decrease, but less than 0.002 Å, and indeed only the Cr1−Cr2 bond distance increases with increasing temperature.

In some unsymmetric systems, the central metal atom has been considered to be disordered over two positions[21,22] due to elongated thermal ellipsoids along the molecular axis. One way to reveal such disorder is by calculating differences of mean square displacement amplitudes, ΔU, along the bond direction.[77−80] In the case of $Co_3(dpa)_4Cl_2$, the thermal ellipsoid of Co3 is elongated along the tricobalt axis, and the atom is considered to be disordered because the ΔU values of Co2−Co3 and Co3−Cl2 bonds are large even at 15 K (>100 × 10^{-4} Å^2). The ΔU values for the Co−N bonds also reflect this disorder although to a minor extent, and they can therefore also be used to reveal positional disorder. In **1**, the ΔU values for the Cr−Cr bonds are around 100 × 10^{-4} Å^2 at 100 K, Figure 2, but they decrease to less

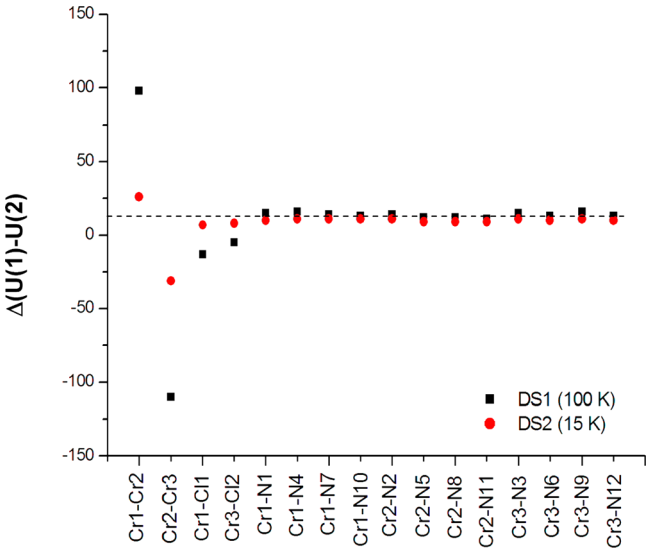

Figure 2. Differences of mean square displacement amplitudes for the bonds involving the Cr atoms (in units of 10^{-4} Å^2).

than 30 × 10^{-4} Å^2 at 15 K. Moreover, the ΔU values of all Cr−N bonds are less than 20 × 10^{-4} Å^2 at both temperatures. This indicates that the central Cr position is not disordered, but has large vibrational amplitude along the metal chain. This is also corroborated by calculating a Fourier difference density map with Cr2 omitted from the model. Such a map only shows one peak at the Cr2 position. We therefore conclude that the elongated thermal ellipsoid of Cr2 is due to this atom sitting in a shallow potential surface (see Supporting Information).

Electron Density Maps. The Laplacian density maps of selected planes containing the Cr atoms are shown in Figure 3. The valence shell charge concentrations (VSCC) and valence shell charge depletions (VSCD) of the M-shell of the Cr atoms are clearly observed. Four VSCCs and four VSCDs are found around each Cr atom in this plane with the VSCCs located in between the Cr−N bond directions. The distributions of the VSCCs of the three Cr atoms are quite similar. The nonspherical Laplacian distributions of the valence shell of the Cr atoms are due to unevenly occupied d orbitals (formally Cr^{2+}, $3d^4$). The VSCCs due to the lone pairs on the N atoms point to the VSCDs of the Cr atoms in a typical key-lock approach, and this supports the coordination bond characters of the Cr−N bonds.[33,46,80−83] The results obtained separately from DS1 and DS2 are clearly consistent. For comparison the theoretical results based on the experimental DS2 structure are also shown in Figure 3, and good agreement is observed between experiment and theory.

Bond Characterization. Selected topological properties of the dpa ligand are listed in Table 3. There are three different types of intraligand bonds in the form of C−C and two types of N−C bonds (pyridine or amine group). The experimental and theoretical topological properties at the BCPs agree well. All of these bonds show large values of ρ_b (~2.3 e Å^{-3}), large negative values of $\nabla^2\rho_b$ (~ −20 e Å^{-5}), and large negative values of H_b (−2 to −3 H Å^{-3}). The position of the BCP is at the midpoint of the C−C bond, but it shifts away from the geometrical center toward the C atom for the N−C bonds due to the polarized character of these bonds. The results are comparable to the values obtained for the neutral ligand.[84]

The most interesting interactions are between the Cr atoms. Selected experimental and theoretical topological properties of the Cr−Cr and Cr−L bond are listed in Table 3. In general, all the topological properties of DS1 and DS2 show comparable results with small ρ_b (<1 e Å^{-3}), positive $\nabla^2\rho_b$, and negative H_b values. The topological properties of the Cr−Cr bonds are similar for the two different experimental data sets despite the differences in the bond distances at the two different temperatures. Larger values of ρ_b at the Cr−Cr BCPs are obtained from theory (~0.46 e Å^{-3} compared with 0.3 e Å^{-3}). Positive values of $\nabla^2\rho_b$ are obtained for all the Cr−Cr bonds, and the sign of H_b is negative for all models indicating covalent bond character. However, the theoretical value is larger (−0.2 H Å^{-3} compared with −0.01 H Å^{-3}). The position of the BCP in the Cr−Cr bonds of DS1 is found at the middle of the bonds, but

dx.doi.org/10.1021/ic501603x | Inorg. Chem. 2014, 53, 12489−12498

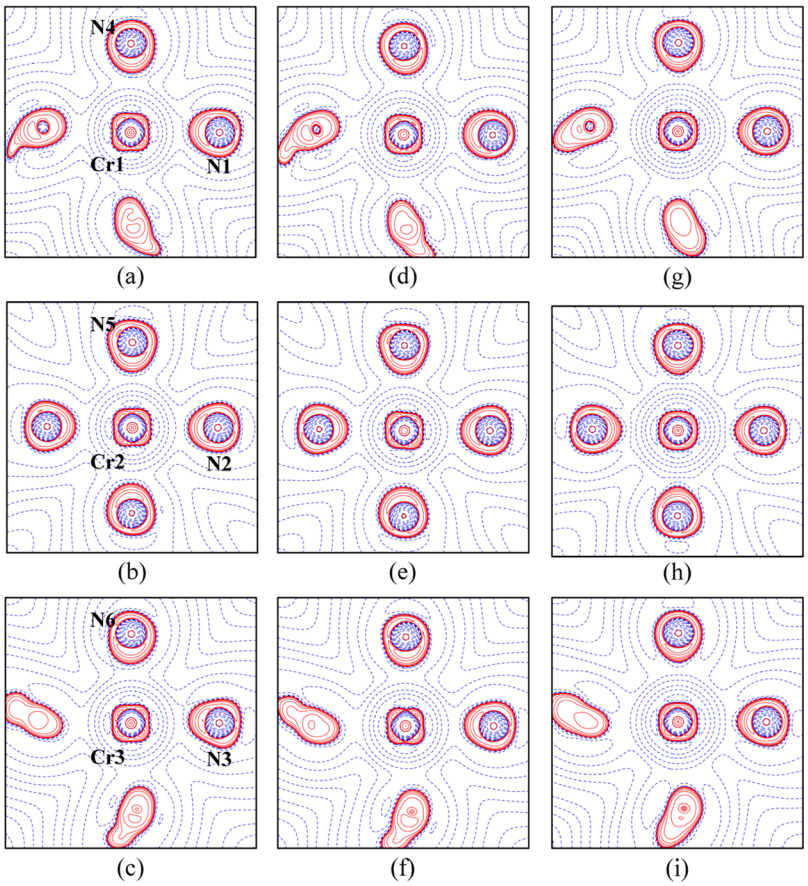

Figure 3. Laplacian distribution of Cr atoms of DS1 (a–c), DS2 (d–f), and theoretical results based on 15 K structure (g–i). The contours are plotted in steps of $(-1)^l 2^m 10^n$ (l = 1, 0; m = 1 to 3; n = −3 to +3) with positive being dashed blue lines and negative solid red lines.

for DS2 it is shifted about 0.04 Å away from Cr2 toward Cr1/Cr3, and this indicates a slightly polarized Cr–Cr bond at 15 K. However, in the theoretical calculation the position of the BCP is almost exactly at the midpoint of the Cr–Cr bonds. The difference between the two experimental densities probably is caused by the fact that in the multipole model Cr2 is less contracted (κ = 1.04) at 15 K than at 100 K (κ = 1.09), while the other Cr atoms are unchanged (κ = 1.13 at 100 K and κ = 1.12 at 15 K). In $Co_3(dpa)_4Cl_2$,[80] which is unsymmetric with Co–Co bond distances of 2.295 and 2.446 Å, the ρ_b values of the two Co–Co bonds are 0.32 and 0.20 e Å^{-3}, respectively. On the basis of the topological analysis, the two Cr–Cr bonds can be classified as transit closed-shell interactions with a value of $|V_b|/G_b \sim 1.6$ from DFT results and 1.0 from experiment. For comparison, the experimental values of two Co–Co bonds in $Co_3(dpa)_4Cl_2$ are 1.0 and 0.90.[80] For **1** the discrepancy between theory and experiment is caused by a difference in the values of V_b, while G_b values are almost identical.

The topological properties of the Cr–L bonds, including Cr–Cl and Cr–N, have common trends. Cr2–N2 has larger ρ_b (~0.60 e Å^{-3}) and more negative H_b (−0.10 H A^{-3}) than the Cr1–N1 and Cr3–N3 bonds ($\rho_b \sim 0.50$ e Å^{-3} and $H_b \sim -0.05$ H A^{-3}) indicating that the Cr2–N2 bond is slightly stronger and more covalent than the others. This is in good agreement with the DFT results. The topological properties of the Cr2–N2 bond are comparable with those observed in $Cr_2(dipp)_2$ (dipp = (Ar)NC(H)N(Ar) and Ar = 2,6-i-Pr_2–C_6H_3; $\rho_b \sim 0.62$ e Å^{-3}, $H_b \sim -0.1$ H A^{-3}).[33] The topological properties of the Cr–Cl bonds are $\rho_b \sim 0.28$ e Å^{-3} and $H_b \sim -0.02$ H A^{-3} again in good agreement with theory (0.32 e Å^{-3} and −0.06 H A^{-3}). The M–L bond is usually considered as a coordination bond (donor–acceptor bond), which was supported by the Laplacian distribution shown above. In some cases covalent bond contributions revealed by the negative sign of H_b have been confirmed by the Fermi hole distribution,[46,81,82,87] and the M–L bond may more appropriately considered a polar covalent bond. The observation of a BCP shift relative to an IAM model supports the polarized bond character. The Laplacian distributions from the IAM and multipole models along the Cr–N and Cr–Cl bond paths are shown in Figure 4. They clearly indicate increased charge accumulation in the valence shell of the coordinated atoms (N and Cl) and charge depletion on the metal valence shell due to the more electronegative N and Cl. This is accompanied by a movement of the BCP toward the Cr atoms in all Cr–L interactions. The BCP shifts 0.023 Å for Cr1–Cl1 and 0.047 Å for Cr1–N1 as depicted in Figure 4. In summary, the Cr–L bonds of **1** can be considered as polar covalent bonds.[33−36,39,46,47,80−83,87−96]

The delocalization index (DI), which cannot be obtained from the experimental multipole model since it requires the pair density, is defined as the average number of electron pairs delocalized (shared) between any pair of atoms, not restricted to those connected through a bond path.[97] In the present case the values of the DI of the two Cr–Cr bonds are ~0.8 while it is 0.5 for all Cr–L bonds. The DI between Cr1 and Cr3 is 0.08.

Source Function. The SF was recently developed by Bader and Gatti,[98,99] and it is a novel descriptor to analyze chemical bonding. Through the SF the electron density at the BCP (ρ_b)

dx.doi.org/10.1021/ic501603x | Inorg. Chem. 2014, 53, 12489−12498

Table 3. Topological Properties of Selected Bonds[a]

bond	DS	model	ρ_b, e Å^{-3}	$\nabla^2\rho_b$, e Å^{-3}	R_{ij}, Å	d_1, Å	λ_1, e Å^{-3}	λ_3, H A^{-3}	G_b,[d] H A^{-3}	H_b,[d] H A^{-3}
Cr1−Cr2	DS1	MM	0.313(1)	4.644(4)	2.348	1.177	−1.020	6.650	0.33	−0.01
		DFT	0.479	2.015	2.348	1.174	−1.738	5.486	0.34	−0.20
	DS2	MM	0.310(0)	4.528(3)	2.367	1.164	−0.990	6.480	0.33	−0.01
		DFT	0.463	1.845	2.368	1.183	−1.664	5.168	0.32	−0.19
Cr2−Cr3	DS1	MM	0.298(1)	4.210(4)	2.377	1.194	−0.910	6.000	0.30	−0.01
		DFT	0.452	1.746	2.378	1.190	−1.626	4.993	0.31	−0.18
	DS2	MM	0.306(0)	4.300(3)	2.369	1.204	−0.940	6.170	0.31	−0.01
		DFT	0.460	1.804	2.370	1.186	−1.658	5.115	0.31	−0.19
Cr−Cr[b]			0.237	2.790	2.4991[c]			4.03		−0.007
(metallic Cr)			0.145	0.926	2.8857[c]			1.00		−0.010
Cr1−Cl1	DS1	MM	0.268(3)	3.191(4)	2.549	1.172	−0.910	4.960	0.24	−0.02
		DFT	0.303	2.757	2.548	1.167	−0.967	4.690	0.25	−0.05
	DS2	MM	0.274(3)	3.474(4)	2.535	1.174	−0.900	5.270	0.26	−0.01
		DFT	0.312	2.864	2.534	1.161	−1.001	4.866	0.26	−0.06
Cr1−N1	DS1	MM	0.508(5)	7.251(8)	2.121	1.023	−2.320	11.530	0.55	−0.04
		DFT	0.483	7.164	2.121	1.015	−2.086	11.164	0.55	−0.05
	DS2	MM	0.490(5)	6.982(6)	2.119	1.041	−2.310	11.310	0.54	−0.05
		DFT	0.485	7.196	2.119	1.014	−2.100	11.223	0.56	−0.05
Cr2−N2	DS1	MM	0.616(6)	8.687(11)	2.038	1.000	−2.960	14.210	0.70	−0.09
		DFT	0.580	8.917	2.039	0.985	−2.777	14.115	0.71	−0.09
	DS2	MM	0.598(6)	8.208(8)	2.036	1.006	−2.940	13.550	0.67	−0.10
		DFT	0.583	8.977	2.037	0.984	−2.800	14.217	0.72	−0.09
N1−C5 (pyridine)	DS1	MM	2.34(2)	−19.59(9)	1.364	0.772	−20.160	17.370	1.41	−2.78
		DFT	2.203	−25.469	1.364	0.859	−17.158	6.530	1.53	−3.32
	DS2	MM	2.49(3)	−21.55(9)	1.363	0.751	−21.830	19.040	1.48	−2.99
		DFT	2.209	−25.471	1.362	0.859	−17.215	6.645	1.56	−3.35
N2−C5 (amine)	DS1	MM	2.21(2)	−15.23(8)	1.375	0.759	−18.220	18.630	1.46	−2.53
		DFT	2.150	−24.940	1.374	0.842	−16.605	6.161	1.25	−2.99
	DS2	MM	2.33(3)	−18.61(9)	1.370	0.743	−20.130	18.970	1.43	−2.73
		DFT	2.164	−25.238	1.370	0.843	−16.737	6.114	1.29	−3.06
C1−C2	DS1	MM	2.27(2)	−20.11(7)	1.381	0.698	−18.600	13.440	1.16	−2.57
		DFT	2.151	−20.765	1.379	0.702	−15.894	8.245	0.73	−2.18
	DS2	MM	2.24(3)	−20.51(8)	1.380	0.692	−18.210	12.680	1.11	−2.55
		DFT	2.152	−20.784	1.379	0.702	−15.905	8.247	0.73	−2.19

[a]The first line is from the experimental multipole model, and the second line is from theory (DFT in the experimental geometry). R_{ij} is the bond path length between bonded atom i and j, d_1 is the bond path length from the BCP to atom I, G_b is the kinetic energy density at the BCP, and H_b is total energy density at the BCP. [b]Cr−Cr bonds in chromium metal based on γ-ray diffraction results.[85] [c]Cr−Cr bond distance in Cr metal. [d]The experimental values are obtained using Abramov's approximation[86] while theoretical values are calculated directly from the wave function using AIMAll.

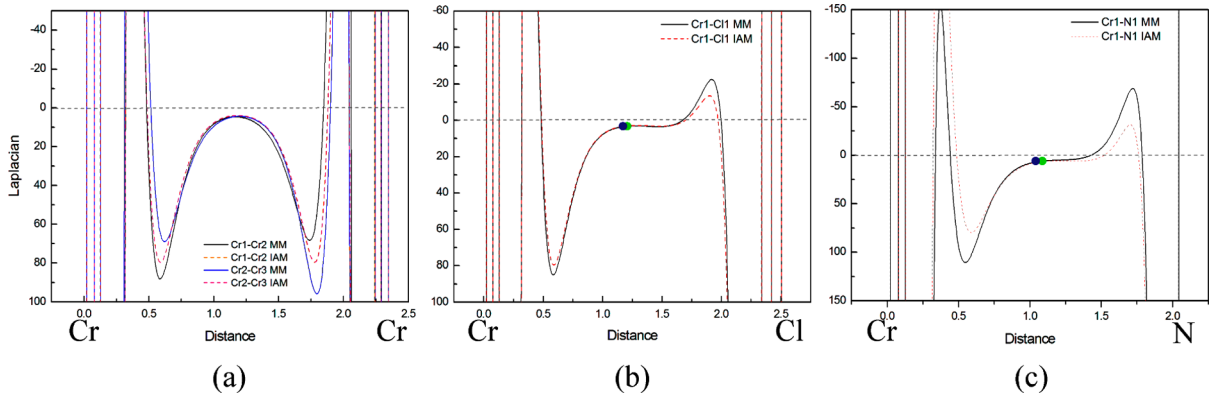

Figure 4. Laplacian distributions (DS2) along Cr−Cr, Cr1−N1, and Cr1−Cl1 bonds. The solid line is from the multipole model (MM), and the dashed line is from the independent atom model (IAM). Blue dots indicate the BCP from MM, and green dots are from the IAM.

and indeed at all points can be regarded as the sum of contributions from individual atoms,[42,51] and it has the major advantage that it can be calculated from an experimental density. As listed in Table 4 and Supporting Information Table S4, there are large discrepancies between the experimental and theoretical SF values. For the Cr1−Cr2 bond, the major experimental SF contributions are from Cr1 (∼10%), Cl1 (∼10%), and all the nitrogen atoms (∼6%). Surprisingly, the

dx.doi.org/10.1021/ic501603x | Inorg. Chem. 2014, 53, 12489−12498

Table 4. SF (%) of Selected Bond

bond	DS	model	ρ_b (e Å^{-3})	Cr1	Cr2	Cr3
Cr1−Cr2	DS1	MM	0.31	9.91	1.15	0.23
		DFT	0.48	30.10	26.97	0.58
	DS2	MM	0.31	11.15	0.21	0.35
		DFT	0.46	29.39	26.21	0.62
Cr2−Cr3	DS1	MM	0.30	0.86	3.37	8.24
		DFT	0.45	0.71	25.51	28.69
	DS2	MM	0.31	0.63	4.30	11.67
		DFT	0.46	0.64	25.87	28.79

bonded Cr2 atom contributes only 1% to this bond. Similar results are observed for Cr2−Cr3. Summation of contribution of all Cr, Cl, and N atoms is 100%. In the theoretical density the bonded Cr atoms each contribute as much as 25−30% to the Cr−Cr bonds. The effect on the SF values of using different basis sets was found to be negligible, in accordance with the findings of Monza et al.[100]

The large discrepancies between experimental and theoretical values are probably due to subtle differences of the Laplacian distribution within each atomic basin. The differences of the Laplacian distribution may be attributable to data quality, systematic errors, and flexibility of the multipole model, and we believe that in the present case the theoretical SF results are more reliable than the experimental ones. A large contribution from the two bonded Cr atoms to Cr−Cr bonds indicates localization of the Cr−Cr bonds in contrast to a delocalized three-center bond.

NBO Analysis. There are no bonding NBOs between the Cr atoms in **1**, but a number of donor−acceptor interactions are found. The dominating (in terms of $E(2)$) Cr−Cr donor−acceptor interactions are listed in Table 5. Each interaction is described in terms of a Lewis-type donor NBO, a non-Lewis-type acceptor NBO, and orbital occupancies. Such analyses have been applied in studies of metal−metal,[33] metal−ligand,[33,46,87,101] and hydrogen bonds.[102−104] The lone pair of Cr1 (LP(4)Cr1) acts as a donor, and the unoccupied lone pair of Cr2 (LP*(1)Cr2) acts as an acceptor for the α electrons. Correspondingly, the lone pair of Cr2 (LP(4)Cr2) acts as a donor, and the unoccupied lone pair of Cr1 (LP*(1)Cr1) acts as an acceptor for the β electrons. These interactions contribute with a significant stabilization energy, $E(2)$ of 180 kcal mol^{-1} from the α electrons and 15 kcal mol^{-1} from the β electrons, respectively. Cr2 and Cr3 show similar donor−acceptor interactions as shown in Table 5. The NBOs of interest in these donor−acceptor interactions are all dominated by the d_{z^2} natural atomic orbital (NAO) resulting in donor−acceptor interactions along the Cr−Cr interatomic axes. The three d_{z^2} NAOs on the Cr atoms are shown in Figure 5.

Atomic Properties of Cr. The atomic properties such as atomic volume, atomic charge, and atomic dipole moment can be obtained from electron density analysis by integrating the atomic basin defined by a zero flux surface, $\nabla\rho \rightarrow (r)\cdot n \rightarrow (r) = 0$,

Table 5. Selected Cr−Cr Donor and Acceptor NBOs and Associated Stabilization Energies, $E(2)$'s, of 1[a]

symmetry	donor(i) occ	acceptor(j) occ	$E(2)$ (kcal mol^{-1})	donor(i) occ	acceptor(j) occ	$E(2)$ (kcal mol^{-1})
	Cr1−Cr2			Cr2−Cr3		
α	LP(4)Cr1	LP*(1)Cr2		LP(4)Cr3	LP*(1)Cr2	
NHO	($s^{2.9\%}p^{4.0\%}d^{93.2\%}$)	($s^{11.0\%}d^{89.0\%}$)		($s^{2.6\%}p^{4.4\%}d^{93.0\%}$)	($s^{11.0\%}d^{89.0\%}$)	
NAO[b]	($3d_{z^2}$)	($3d_{z^2}$)		($3d_{z^2}$)	($3d_{z^2}$)	
DS1	0.820 73	0.483 49	185.38	0.819 24	0.483 49	211.36
DS2	0.823 61	0.481 75	172.90	0.817 06	0.481 75	172.09
β	LP(4)Cr2	LP*(1)Cr1		LP(4)Cr2	LP*(1)Cr3	
NHO	($s^{7.0\%}d^{93.0\%}$)	($s^{1.9\%}p^{0.3\%}d^{97.8\%}$)		($s^{7.0\%}d^{93.0\%}$)	($s^{2.0\%}p^{0.2\%}d^{97.8\%}$)	
NAO[b]	($3d_{z^2}$)	($3d_{z^2}$)		($3d_{z^2}$)	($3d_{z^2}$)	
DS1	0.770 97	0.278 93	15.53	0.770 97	0.272 57	13.63
DS2	0.770 10	0.275 80	14.95	0.770 10	0.276 26	14.64

[a]Natural hybrid orbital (NHO) compositions and dominating natural atomic orbitals listed in parentheses: LP lone pair (Lewis type), LP* lone pair (non-Lewis type). The listed donor−acceptor interactions have the highest $E(2)$ energy in each interaction. Only the NHO compositions of DS1 are listed. Those of DS2 are similar to DS1. [b]Dominating NAO to the NHO.

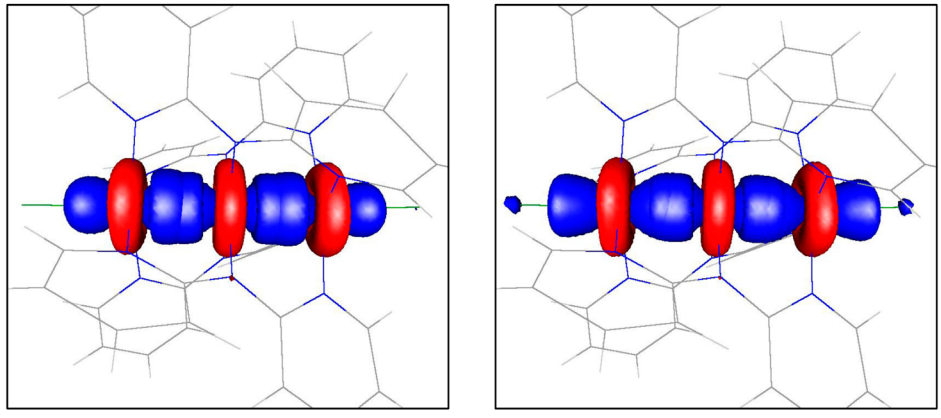

Figure 5. Three d_{z^2} NAOs on the Cr atoms of (a) DS1 and (b) DS2. Blue and red surfaces represent positive and negative isosurfaces.

dx.doi.org/10.1021/ic501603x | Inorg. Chem. 2014, 53, 12489−12498

where $n \rightarrow (r)$ is the vector normal to the surface. Selected atomic properties of the Cr atoms are listed in Supporting Information Table S6. The two data sets show consistent trends but disagree on some points. The integrated number of electrons of the Cr atoms is about 23*e*. The atomic volumes are similar, but the two terminal Cr atoms have slightly larger volume than Cr2. The atomic volume of Cr2 atom is a little larger at 15 K than 100 K due to smaller κ value (1.04) at 15 K. The smaller volume of the Cr2 atom compared with Cr1 and Cr3 is primarily due to the shorter Cr−N bond distance. The average bond path length (bcp to Cr atom) of Cr−N is 1.03 (1.05 in DS2) Å for Cr1/Cr3−N, and it is 1.00 (1.01 in DS2) Å for Cr2−N (see Supporting Information Tables S1−S2).

CONCLUSION

The metal−metal bond plays an important role in forming a metal wire with the electrons being part of the conducting path. Trichromium metal string has the highest conductivity in trimetal wires. The molecular structure of **1** can be considered as a structurally symmetric form due to the small difference in bond length (<0.02 Å) between two Cr−Cr bonds. According to the topological analyses, the Cr−Cr bonds have some covalent bond character and small polarization at 15 K. The SF indicates that the Cr atoms contribute electron density to Cr−Cr bonds. Moreover, the delocalization index of each Cr−Cr bond is 0.8 indicating a single bond. The Cr−Cr bond is described by NBO analyses to exhibit donor−acceptor interactions along the metal-chain axes. The topological properties at the Cr−Cr bond critical points indicate covalently bond characters which have comparable topological properties to the Cr−Cr bond in Cr metal.

Generally, the topological properties of **1** are in good agreement between experiment and theory for the intraligand bonds. Overall, they also show similar trends for the Cr−Cr bonds with clear covalent contributions. However, some discrepancies of topological properties are observed between experimental and theoretical results, such as the values of ρ_b, H_b, SF, as well as the atomic charge and the atomic dipole moment of the Cr atoms.

ASSOCIATED CONTENT

Supporting Information

Residual and deformation density maps, theoretical potential energy curve, full topological analysis, complete source function contributions, integrated atomic properties, d-orbital populations, and DMSDA tables. This material is available free of charge via the Internet at http://pubs.acs.org.

AUTHOR INFORMATION

Corresponding Authors

*E-mail: jacobo@chem.au.dk.
*E-mail: bo@chem.au.dk.

Notes

The authors declare no competing financial interest.

ACKNOWLEDGMENTS

We gratefully acknowledge the beam time obtained at beamline 15-ID-E, ChemMatCARS beamline, The University of Chicago, Advanced Photon Source. The work was supported by the Danish Research Council (Danscatt) and by the Danish National Research Foundation (DNRF93)

REFERENCES

(1) Joachim, C.; Gimzewski, J. K.; Aviram, A. *Nature* **2000**, *408*, 541−548.
(2) Lin, S. Y.; Chen, I. W. P.; Chen, C. H.; Hsieh, M. H.; Yeh, C. Y.; Lin, T. W.; Chen, Y. H.; Peng, S. M. *J. Phys. Chem. B* **2004**, *108*, 959−964.
(3) Chen, I. W. P.; Fu, M.-D.; Tseng, W.-H.; Yu, J.-Y.; Wu, S.-H.; Ku, C.-J.; Chen, C.-h.; Peng, S.-M. *Angew. Chem., Int. Ed.* **2006**, *45*, 5814−5818.
(4) Tsai, T.-W.; Huang, Q.-R.; Peng, S.-M.; Jin, B.-Y. *J. Phys. Chem. C* **2010**, *114*, 3641−3644.
(5) Wu, L. P.; Field, P.; Morrissey, T.; Murphy, C.; Nagle, P.; Hathaway, B.; Simmons, C.; Thornton, P. *J. Chem. Soc., Dalton Trans.* **1990**, 3835−3840.
(6) Pyrka, G. J.; Elmekki, M.; Pinkerton, A. A. *J. Chem. Soc., Chem. Commun.* **1991**, 84−85.
(7) Clérac, R.; Cotton, F. A.; Dunbar, K. R.; Hillard, E. A.; Petrukhina, M. A.; Smucker, B. W. *C. R. Acad. Sci. Paris, Chim.* **2001**, *4*, 315−319.
(8) Berry, J. F.; Cotton, F. A.; Lei, P.; Murillo, C. A. *Inorg. Chem.* **2003**, *42*, 377−382.
(9) Berry, J. F.; Cotton, F. A.; Daniels, L. M.; Murillo, C. A.; Wang, X. P. *Inorg. Chem.* **2003**, *42*, 2418−2427.
(10) Hurley, T. J.; Robinson, M. A. *Inorg. Chem.* **1968**, *7*, 33−&.
(11) Aduldecha, S.; Hathaway, B. *J. Chem. Soc., Dalton Trans.* **1991**, 993−998.
(12) Peng, C. H.; Wang, C. C.; Lee, H. C.; Lo, W. C.; Lee, G. H.; Peng, S. M. *J. Chin. Chem. Soc. (Taipei, Taiwan)* **2001**, *48*, 987−996.
(13) Zhu, L. G.; Peng, S. M.; Lee, G. H. *Chem. Lett.* **2002**, 1210−1211.
(14) Zhu, L. G.; Peng, S. M.; Lee, G. H. *Anal. Sci.* **2002**, *18*, 1067−1068.
(15) Li, H.; Lee, G. H.; Peng, S. M. *Inorg. Chem. Commun.* **2003**, *6*, 1−4.
(16) Clérac, R.; Cotton, F. A.; Dunbar, K. R.; Murillo, C. A.; Pascual, I.; Wang, X. P. *Inorg. Chem.* **1999**, *38*, 2655−2657.
(17) Yang, E. C.; Cheng, M. C.; Tsai, M. S.; Peng, S. M. *J. Chem. Soc., Chem. Commun.* **1994**, 2377−2378.
(18) Clérac, R.; Cotton, F. A.; Daniels, L. M.; Dunbar, K. R.; Kirschbaum, K.; Murillo, C. A.; Pinkerton, A. A.; Schultz, A. J.; Wang, X. P. *J. Am. Chem. Soc.* **2000**, *122*, 6226−6236.
(19) Cotton, F. A.; Daniels, L. M.; Murillo, C. A.; Pascual, I. *J. Am. Chem. Soc.* **1997**, *119*, 10223−10224.
(20) Clérac, R.; Cotton, F. A.; Daniels, L. M.; Dunbar, K. R.; Murillo, C. A.; Pascual, I. *Inorg. Chem.* **2000**, *39*, 748−751.
(21) Clérac, R.; Cotton, F. A.; Daniels, L. M.; Dunbar, K. R.; Murillo, C. A.; Pascual, I. *Inorg. Chem.* **2000**, *39*, 752−756.
(22) Berry, J. F.; Cotton, F. A.; Lu, T. B.; Murillo, C. A.; Roberts, B. K.; Wang, X. P. *J. Am. Chem. Soc.* **2004**, *126*, 7082−7096.
(23) Hsiao, C. J.; Lai, S. H.; Chen, I. C.; Wang, W. Z.; Peng, S. M. *J. Phys. Chem. A* **2008**, *112*, 13528−13534.
(24) Huang, Y. M.; Tsai, H. R.; Lai, S. H.; Lee, S. J.; Chen, I. C.; Huang, C. L.; Peng, S. M.; Wang, W. Z. *J. Phys. Chem. C* **2011**, *115*, 13919−13926.
(25) Chen, Y. H.; Lee, C. C.; Wang, C. C.; Lee, G. H.; Lai, S. Y.; Li, F. Y.; Mou, C. Y.; Peng, S. M. *Chem. Commun.* **1999**, 1667−1668.
(26) Benbellat, N.; Rohmer, M. M.; Bénard, M. *Chem. Commun.* **2001**, 2368−2369.
(27) Rohmer, M. M.; Bénard, M. *J. Am. Chem. Soc.* **1998**, *120*, 9372−9373.
(28) Rohmer, M. M.; Bénard, M. *Chem. Soc. Rev.* **2001**, *30*, 340−354.
(29) Rohmer, M. M.; Strich, A.; Bénard, M.; Malrieu, J. P. *J. Am. Chem. Soc.* **2001**, *123*, 9126−9134.
(30) Bader, R. F. W. *Atoms in Molecules: a Quantum Theory*; Clarendon Press: Oxford, 1990.
(31) Espinosa, E.; Alkorta, I.; Elguero, J.; Molins, E. *J. Chem. Phys.* **2002**, *117*, 5529−5542.
(32) Gervasio, G.; Bianchi, R.; Marabello, D. *Chem. Phys. Lett.* **2004**, *387*, 481−484.

(33) Wu, L.-C.; Hsu, C.-W.; Chuang, Y.-C.; Lee, G.-H.; Tsai, Y.-C.; Wang, Y. *J. Phys. Chem. A* **2011**, *115*, 12602−12615.
(34) Macchi, P.; Proserpio, D. M.; Sironi, A. *J. Am. Chem. Soc.* **1998**, *120*, 13429−13435.
(35) Bianchi, R.; Gervasio, G.; Marabello, D. *Inorg. Chem.* **2000**, *39*, 2360−2366.
(36) Farrugia, L. J.; Mallinson, P. R.; Stewart, B. *Acta Crystallogr., Sect. B* **2003**, *59*, 234−247.
(37) Mitschler, A.; Rees, B.; Wiest, R.; Bénard, M. *J. Am. Chem. Soc.* **1982**, *104*, 7501−7509.
(38) Hino, K.; Saito, Y.; Bénard, M. *Acta Crystallogr., Sect. B* **1981**, *37*, 2164−2170.
(39) Macchi, P.; Sironi, A. *Coord. Chem. Rev.* **2003**, *238*, 383−412.
(40) Bianchi, R.; Gervasio, G.; Marabello, D. *Chem. Commun.* **1998**, 1535−1536.
(41) Gotz, K.; Kaupp, M.; Braunschweig, H.; Stalke, D. *Chem.—Eur. J.* **2009**, *15*, 623−632.
(42) Gatti, C.; Lasi, D. *Faraday Discuss.* **2007**, *135*, 55−78.
(43) Savin, A.; Nesper, R.; Wengert, S.; Fassler, T. F. *Angew. Chem., Int. Ed.* **1997**, *36*, 1809−1832.
(44) Ponec, R.; Yuzhakov, G.; Sundberg, M. R. *J. Comput. Chem.* **2005**, *26*, 447−454.
(45) Ponec, R.; Feixas, F. *J. Phys. Chem. A* **2009**, *113*, 8394−8400.
(46) Wang, C. C.; Tang, T. H.; Wang, Y. *J. Phys. Chem. A* **2000**, *104*, 9566−9572.
(47) Overgaard, J.; Clausen, H. F.; Platts, J. A.; Iversen, B. B. *J. Am. Chem. Soc.* **2008**, *130*, 3834−3843.
(48) Overgaard, J.; Jones, C.; Stasch, A.; Iversen, B. B. *J. Am. Chem. Soc.* **2009**, *131*, 4208−4209.
(49) Overgaard, J.; Platts, J. A.; Iversen, B. B. *Acta Crystallogr., Sect. B* **2009**, *65*, 715−723.
(50) Gatti, C. *Z. Kristallogr.* **2005**, *220*, 399−457.
(51) Gatti, C.; Cargnoni, F.; Bertini, L. *J. Comput. Chem.* **2003**, *24*, 422−436.
(52) Li, H.; Lee, G. H.; Peng, S. M. *J. Mol. Struct.* **2004**, *707*, 179−186.
(53) *SAINT*; Bruker AXS Inc.: Madison, WI, 2005.
(54) Sheldrick, G. M. *Program SADABS*; University of Göttingen: Göttingen, Germany, 1997.
(55) Blessing, R. H. *J. Appl. Crystallogr.* **1997**, *30*, 421−426.
(56) Hardie, M. J.; Kirschbaum, K.; Martin, A.; Pinkerton, A. A. *J. Appl. Crystallogr.* **1998**, *31*, 815−817.
(57) Zaleski, J.; Wu, G.; Coppens, P. *J. Appl. Crystallogr.* **1998**, *31*, 302−304.
(58) Wu, G.; Rodrigues, B. L.; Coppens, P. *J. Appl. Crystallogr.* **2002**, *35*, 356−359.
(59) Sheldrick, G. M. *SHELXS-97, Program for Solution of Crystal Structures*; University of Göttingen: Göttingen, Germany, 1997.
(60) Volkov, A. P. M.; Farrugia, L. J.; Gatti, C.; Mallinson, P.; Richter, T.; Koritsanszky, T. *XD2006—A Computer Program for Multipole Refinement, Topological Analysis of Charge Densities, Evaluation of Intermolecular Energies from Experimental or Theoretical Structure Factors*; 2006.
(61) Hansen, N. K.; Coppens, P. *Acta Crystallogr., Sect. A* **1978**, *34*, 909−921.
(62) Schmøkel, M. S.; Bjerg, L.; Larsen, F. K.; Overgaard, J.; Cenedese, S.; Christensen, M.; Madsen, G. K. H.; Gatti, C.; Nishibori, E.; Sugimoto, K.; Takata, M.; Iversen, B. B. *Acta Crystallogr., Sect. A* **2013**, *69*, 570−582.
(63) Müller, P.; Herbst-Irmer, R.; Spek, A.; Schneider, T.; Sawaya, M. *Crystal Structure Refinement: A Crystallographer's Guide to SHELXL (International Union of Crystallography Texts on Crystallography)*; Oxford University Press: New York, 2006.
(64) Steiner, T. *Angew. Chem., Int. Ed.* **2002**, *41*, 48−76.
(65) Frisch, M. J.; Trucks, G. W.; Schlegel, H. B.; Scuseria, G. E.; Robb, M. A.; Cheeseman, J. R.; Scalmani, G.; Barone, V.; Mennucci, B.; Petersson, G. A.; Nakatsuji, H.; Caricato, M.; Li, X.; Hratchian, H. P.; Izmaylov, A. F.; Bloino, J.; Zheng, G.; Sonnenberg, J. L.; Hada, M.; Ehara, M.; Toyota, K.; Fukuda, R.; Hasegawa, J.; Ishida, M.; Nakajima, T.; Honda, Y.; Kitao, O.; Nakai, H.; Vreven, T.; Montgomery, J. A., Jr.; Peralta, J. E.; Ogliaro, F.; Bearpark, M.; Heyd, J. J.; Brothers, E.; Kudin, K. N.; Staroverov, V. N.; Kobayashi, R.; Normand, J.; Raghavachari, K.; Rendell, A.; Burant, J. C.; Iyengar, S. S.; Tomasi, J.; Cossi, M.; Rega, N.; Millam, J. M.; Klene, M.; Knox, J. E.; Cross, J. B.; Bakken, V.; Adamo, C.; Jaramillo, J.; Gomperts, R.; Stratmann, R. E.; Yazyev, O.; Austin, A. J.; Cammi, R.; Pomelli, C.; Ochterski, J. W.; Martin, R. L.; Morokuma, K.; Zakrzewski, V. G.; Voth, G. A.; Salvador, P.; Dannenberg, J. J.; Dapprich, S.; Daniels, A. D.; Farkas, O.; Foresman, J. B.; Ortiz, J. V.; Cioslowski, J.; Fox, D. J. *Gaussian 09, Revision A.02*; Gaussian, Inc.: Wallingford CT, 2009.
(66) Becke, A. D. *J. Chem. Phys.* **1986**, *84*, 4524−4529.
(67) Becke, A. D. *Phys. Rev. A* **1988**, *38*, 3098−3100.
(68) Perdew, J. P. *Phys. Rev. B* **1986**, *34*, 7406−7406.
(69) Perdew, J. P. *Phys. Rev. B* **1986**, *33*, 8822−8824.
(70) Balabanov, N. B.; Peterson, K. A. *J. Chem. Phys.* **2005**, *123*, 064107.
(71) Foster, J. P.; Weinhold, F. *J. Am. Chem. Soc.* **1980**, *102*, 7211−7218.
(72) Reed, A. E.; Weinhold, F. *J. Chem. Phys.* **1983**, *78*, 4066−4073.
(73) Reed, A. E.; Weinstock, R. B.; Weinhold, F. *J. Chem. Phys.* **1985**, *83*, 735−746.
(74) Weinhold, F.; Carpenter, J. E. In *The Structure of Small Molecules and Ions*; Naaman, R., Vager, Z., Eds.; Springer: New York, 1988.
(75) Glendening, E. D.; Reed, A. E.; Carpenter, J. E.; Weinhold, F. *NBO Version 3.1*.
(76) Keith, T. A. *AIMAll (Version 13.01.27)*; TK Gristmill Software: Overland Park, KS, 2012.
(77) Madsen, G. K. H.; Iversen, B. B.; Larsen, F. K.; Kapon, M.; Reisner, G. M.; Herbstein, F. H. *J. Am. Chem. Soc.* **1998**, *120*, 10040−10045.
(78) Herbstein, F. H.; Iversen, B. B.; Kapon, M.; Larsen, F. K.; Madsen, G. K. H.; Reisner, G. M. *Acta Crystallogr., Sect. B* **1999**, *55*, 767−787.
(79) Wilson, C.; Iversen, B. B.; Overgaard, J.; Larsen, F. K.; Wu, G.; Palii, S. P.; Timco, G. A.; Gerbeleu, N. V. *J. Am. Chem. Soc.* **2000**, *122*, 11370−11379.
(80) Poulsen, R. D.; Overgaard, J.; Schulman, A.; Ostergaard, C.; Murillo, C. A.; Spackman, M. A.; Iversen, B. B. *J. Am. Chem. Soc.* **2009**, *131*, 7580−7591.
(81) Lee, C. R.; Wang, C. C.; Chen, K. C.; Lee, G. H.; Wang, Y. *J. Phys. Chem. A* **1999**, *103*, 156−165.
(82) Lee, C. R.; Tan, L. Y.; Wang, Y. *J. Phys. Chem. Solids* **2001**, *62*, 1613−1628.
(83) Poulsen, R. D.; Jorgensen, M. R. V.; Overgaard, J.; Larsen, F. K.; Morgenroth, W. G.; Graber, T.; Chen, Y. S.; Iversen, B. B. *Chem.—Eur. J.* **2007**, *13*, 9775−9790.
(84) Wu, L.-C.; Lee, G.-H.; Chen, C.-K.; Wang, C.-C. *J. Chin. Chem. Soc. (Taipei, Taiwan)* **2013**, *60*, 823−830.
(85) Jauch, W.; Reehuis, M. *Phys. Rev. B* **2006**, *73*, 085102.
(86) Abramov, Y. A. *Acta Crystallogr., Sect. A* **1997**, *53*, 264−272.
(87) Wang, C. C.; Wang, Y.; Liu, H. J.; Lin, K. J.; Chou, L. K.; Chan, K. S. *J. Phys. Chem. A* **1997**, *101*, 8887−8901.
(88) Jansen, G.; Schubart, M.; Findeis, B.; Gade, L. H.; Scowen, I. J.; McPartlin, M. *J. Am. Chem. Soc.* **1998**, *120*, 7239−7251.
(89) Macchi, P.; Schultz, A. J.; Larsen, F. K.; Iversen, B. B. *J. Phys. Chem. A* **2001**, *105*, 9231−9242.
(90) Overgaard, J.; Larsen, F. K.; Schiøtt, B.; Iversen, B. B. *J. Am. Chem. Soc.* **2003**, *125*, 11088−11099.
(91) Pillet, S.; Souhassou, M.; Mathoniere, C.; Lecomte, C. *J. Am. Chem. Soc.* **2004**, *126*, 1219−1228.
(92) Farrugia, L. J.; Evans, C. *C. R. Chim.* **2005**, *8*, 1566−1583.
(93) Macchi, P.; Donghi, D.; Sironi, A. *J. Am. Chem. Soc.* **2005**, *127*, 16494−16504.
(94) Deeken, S.; Motz, G.; Bezugly, V.; Borrmann, H.; Wagner, F. R.; Kempe, R. *Inorg. Chem.* **2006**, *45*, 9160−9162.
(95) Clausen, H. F.; Overgaard, J.; Chen, Y. S.; Lversen, B. B. *J. Am. Chem. Soc.* **2008**, *130*, 7988−7996.

(96) Overgaard, J.; Larsen, F. K.; Timco, G. A.; Iversen, B. B. *Dalton Trans.* **2009**, 664−671.
(97) Fradera, X.; Austen, M. A.; Bader, R. F. W. *J. Phys. Chem. A* **1999**, *103*, 304−314.
(98) Bader, R. F. W.; Gatti, C. *Chem. Phys. Lett.* **1998**, *287*, 233−238.
(99) Gatti, C.; Bertini, L. *Acta Crystallogr., Sect. A* **2004**, *60*, 438−449.
(100) Monza, E.; Gatti, C.; Lo Presti, L.; Ortoleva, E. *J. Phys. Chem. A* **2011**, *115*, 12864−12878.
(101) Wu, L.-C.; Weng, T.-C.; Hsu, I. J.; Liu, Y.-H.; Lee, G.-H.; Lee, J.-F.; Wang, Y. *Inorg. Chem.* **2013**, *52*, 11023−11033.
(102) Reed, A. E.; Weinhold, F.; Curtiss, L. A.; Pochatko, D. J. *J. Chem. Phys.* **1986**, *84*, 5687−5705.
(103) Weinhold, F. *THEOCHEM* **1997**, *398*, 181−197.
(104) Weinhold, F.; Klein, R. A. *Mol. Phys.* **2012**, *110*, 565−579.

■ NOTE ADDED AFTER ASAP PUBLICATION

This paper was published ASAP on November 10, 2014. Table 1 was updated. The revised paper was reposted on November 19, 2014.